J. Cent. South Univ. (2013) 20: 1786−1791
DOI: 10.1007/s11771-013-1673-x

Springer

Microstructure, texture and tensile properties of Mg-10Sn alloys extruded in different conditions

CHENG Wei-li(程伟丽)[1, 2], LI Jia-wei(李家威)[2], QUE Zhong-ping(阙仲萍)[1, 2], ZHANG Jin-shan(张金山)[2], XU Chun-xiang(许春香)[2], LIANG Wei(梁伟)[2], YOU Bong-Sun[3], PARK Sung Soo[4]

1. Key Laboratory of Interface Science and Engineering in Advanced Materials, Ministry of Education, Taiyuan University of Technology, Taiyuan 030024, China;
2. School of Materials Science and Engineering, Taiyuan University of Technology, Taiyuan 030024, China;
3. Korea Institute of Materials Science, Changwon 641-831, Korea;
4. Ulsan National Institute of Science and Technology, Ulsan 689−798, Korea

Abstract: Indirect extrusion of Mg-10%Sn (mass fraction) alloys was performed at three different working temperatures. The effect of working temperature on the microstructure, texture and tensile properties of the extruded alloys was investigated by optical microscope (OM), scanning electronic microscope (SEM), X-ray diffraction (XRD) and a standard universal testing machine. Grain size, area fraction of second phase particles and texture of the alloys are found to be significantly influenced by working temperature. The grain size refinement is greatly dependent on processing conditions with the low working temperature being the most effective. While the high working temperature results in a coarser grain size and a stronger fiber texture and the reason for this phenomenon was examined in terms of second phase particle, grain type and dynamic recrystallization mechanism. Tested in the different conditions, the tensile strengths of the Mg-10Sn alloys extruded at the high working temperature are remarkably better than those of the other studied alloys. This significant improvement in tensile properties is mainly due to the particle strengthening and texture strengthening resulted from the more and finer primary dispersed particles and stronger texture, respectively.

Key words: magnesium alloy; extrusion; microstructure; texture; tensile properties

1 Introduction

Magnesium alloys have a great potential for application in lightweight structural parts owing to their low density, excellent specific strength and stiffness [1]. However, its absolute strength is lower than that of competitive aluminum alloys. Development of high strength Mg alloy is required and grain refinement is a promising way to enhance yield strength based on the Hall-Petch relationship [2−5].

Extrusion process is an effective grain refinement technique for Mg alloys. However, the application of wrought Mg alloys to a conventional direct extrusion is not considered to be cost-effective. The indirect extrusion has many advantages to traditional direct extrusion and it is expected to be a feasible implementation at lower temperature and higher speed. For the development of high-strength wrought magnesium alloy with superior heat resistance, one promising system is a precipitation hardenable Mg-Sn alloy with high melting temperature (770 °C) Mg_2Sn precipitate [6]. However, reports on indirect-extruded Mg-Sn [7−8] alloy have seldom been presented so far despite a few reports on cast ones [9−11].

Previous research [8] studied the microstructure and tensile properties of indirect-extruded Mg-(6−10)%Sn alloys and the results indicate that the Mg-10Sn alloy exhibits the highest tensile strength and extrudability. Therefore, a binary Mg-10Sn alloy was extruded under controlled conditions with three working temperatures and how working temperature influences the microstructure, texture and tensile properties of indirect extruded Mg-10Sn alloys was explored.

2 Experimental

Analyzed composition of the binary Mg-10Sn alloy was Mg-10.2%Sn (mass fraction) (T10). Details of the billet casting procedure have been described elsewhere [8]. After casting, the alloys were homogenized at 500 °C for 3 h and then water-quenched to induce a

Foundation item: Project(2012R1A1A1012802) supported by the National Research Foundation of Korea Funded by the Ministry of Education, Science and Technology; Project(2013021013−4) supported by Shanxi Province Science Foundation for Youths, China; Project(2012L003) supported by Advanced Programs of Department of Human Resources and Social Security of Shanxi Province for Returned Scholars, China; Project supported by Foundation for Young Scholars of Taiyuan University of Technology, China
Received date: 2012−08−21; **Accepted date:** 2012−11−26
Corresponding author: QUE Zhong-ping, Associate Professor; PhD; Tel: +86−351−6010021; E-mail: quezhongping@163.com

supersaturated solid solution. The billets were 80 mm in diameter and 200 mm in length. These billets were extruded at an extrusion ratio of 25 at three different working temperatures. It is difficult to measure the temperature of deforming material directly so that the exit temperature of die was mentioned and defined as the working temperature. Other extrusion parameters, such as initial billet temperature and ram velocity, are controlled to make the working temperature low, medium and high, based on the preliminary extrusion tests. The alloy designations and extrusion conditions [12] are summarized in Table 1. Microstructural and textural examinations were conducted in midsection parallel to the extrusion direction (ED). For microstructure observations, specimens were etched after polishing in acetic picral (5 g picric acid, 5 mL acetic acid, 10 mL H_2O and 100 mL ethanol). The average grain size was analyzed from several micrographs from longitudinal sections using a computer-aided liner intercept measurement. SEM was used to study the morphology and area fraction of the second phase particles. Texture measurements were taken via X-ray diffraction in the back reflection mode with monochromatic Cu K_α radiation.

Table 1 Indirect extrusion conditions and grain sizes of extruded T10 alloys

Alloy	Initial billet temperature/ °C	Ram speed/ ($mm \cdot s^{-1}$)	Reference die exit temperature/°C	Z parameter/ 10^{-11}
T10-L	250	1.3	292	7.7
T10-M	250	6.7	330	1.5
T10-H	300	6.7	391	0.5

Die exit temperature and Z parameter are chosen from data in Ref. [12].

Tensile test was conducted using an Instron 4206 universal testing machine equipped with 10 mm gauge extensometer. All tensile tests were carried out with an initial strain rate of 1×10^{-3} s^{-1} at ambient temperature, where the tensile direction was parallel to the extrusion direction (ED).

3 Results and discussion

Figure 1 shows the microstructures of homogenized T10 alloy investigated in this work. As indicated, the microstructure of a homogenized binary Mg-10Sn alloy consists of α-Mg grains with average grain size of 68 μm and a few Mg_2Sn particles (volume fraction of 1.95%) that remain undissolved after homogenization. Since the equilibrium solid solubility of Sn in Mg at 500 °C is about 9.8% (mass fraction), considerable Mg_2Sn particles are expected to remain in the T10 alloy after homogenization implemented at that temperature.

The optical micrographs of the extruded alloys are revealed in Fig. 2. The extruded alloys show considerably refined equiaxed grain microstructures, which are mainly a consequence of dynamic recrystallization during the extrusion process. The results of the mean linear intercept grain size are listed in Table 2. It is found that the grain size of the alloys is coarsened obviously as the working temperature increases. The average grain sizes are 2.0, 7.9 and 15.2 μm for T10-L, T10-M and T10-H, respectively. Zener-Hollomon (Z) parameter is also calculated using die exit temperature other than initial billet temperature and listed in Table 1. Similar to other reports [12−13], the average grain size (d) is a function of Z, which can be formulated in the typical form as $\ln d=A+B\ln Z$, with A and B values of −16.7 and −0.74, respectively. It should be noted that some row stacked grains (RSGs) are found in the T10-M alloy. It is reported that the formation of RSGs is due to the slow nucleation rate in localized deformation bands. RSGs and fine equiaxed grains are both DRX grains with the former leading to weaker texture [14].

Furthermore, the coarse Mg_2Sn particles (CMPs) are found to be aligned along the ED in the form of stringers after being broken into fragments during the extrusion process. The area fraction of CMPs firstly increases and then decreases with increasing working temperature. The related results are listed in Table 2. The sizes of the CMPs inside the stringers are measured to be more than 1 μm, ranging from 1 to 4.5 μm.

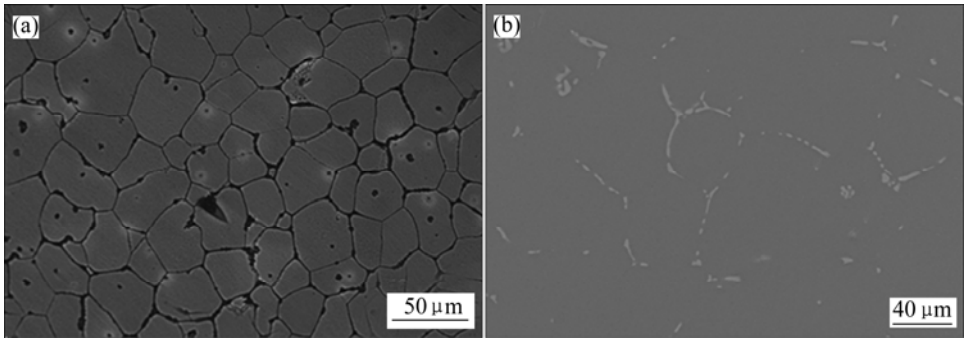

Fig. 1 Micrographs of homogenized Mg-10Sn alloys: (a) OM; (b) SEM

In addition to the CMPs, relatively fine Mg_2Sn particles (FMPs) with sizes of less than 1 μm (Fig. 3), which are not present prior to extrusion, are distributed in the α-Mg matrix. Similar results on the formation of fine particles during extrusion have been reported in precipitation hardenable Mg alloys, and explained to be attributed to dynamic precipitation [3, 7]. The variation in the area fraction of FMPs as a function of working temperature is contrary to that of CMPs. The area fractions of particles decrease firstly and then increase as

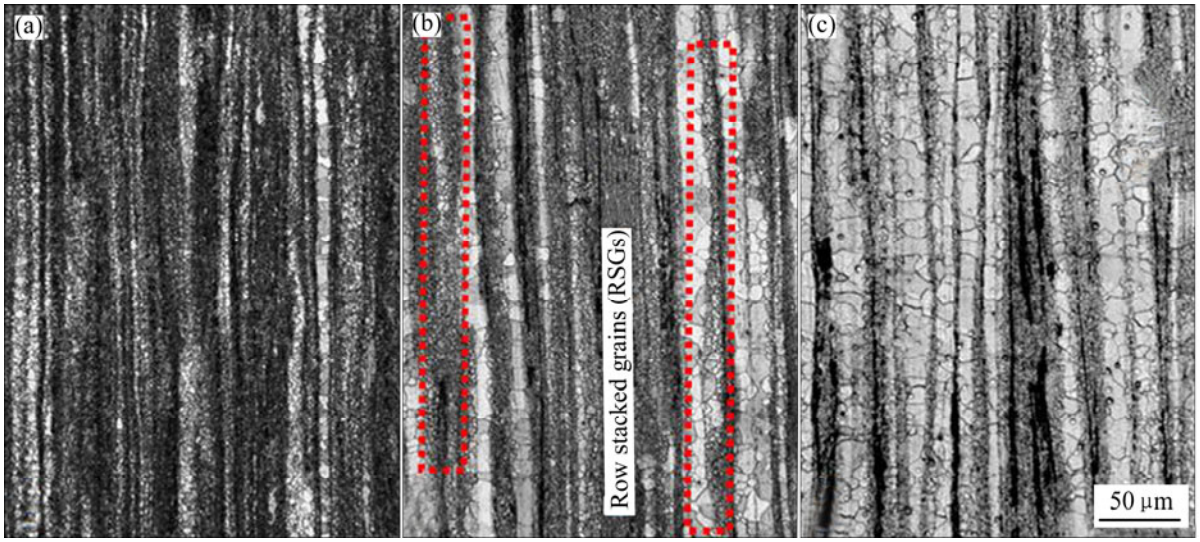

Fig. 2 Optical micrographs of extruded T10 alloys in different conditions: (a) T10-L; (b) T10-M; (c) T10-H

Table 2 Tensile properties and area fraction of second phase particles of studied alloys

Alloy	Average grain size/μm	Fraction of CMPs/%	Fraction of FMPs/%	TYS/MPa	UTS/MPa	Elongation/%
T10-L	2.0	4.43	7.8	237	269	15.0
T10-M	7.9	7.96	6.5	225	263	11.7
T10-H	15.2	1.76	11.6	240	284	12.0

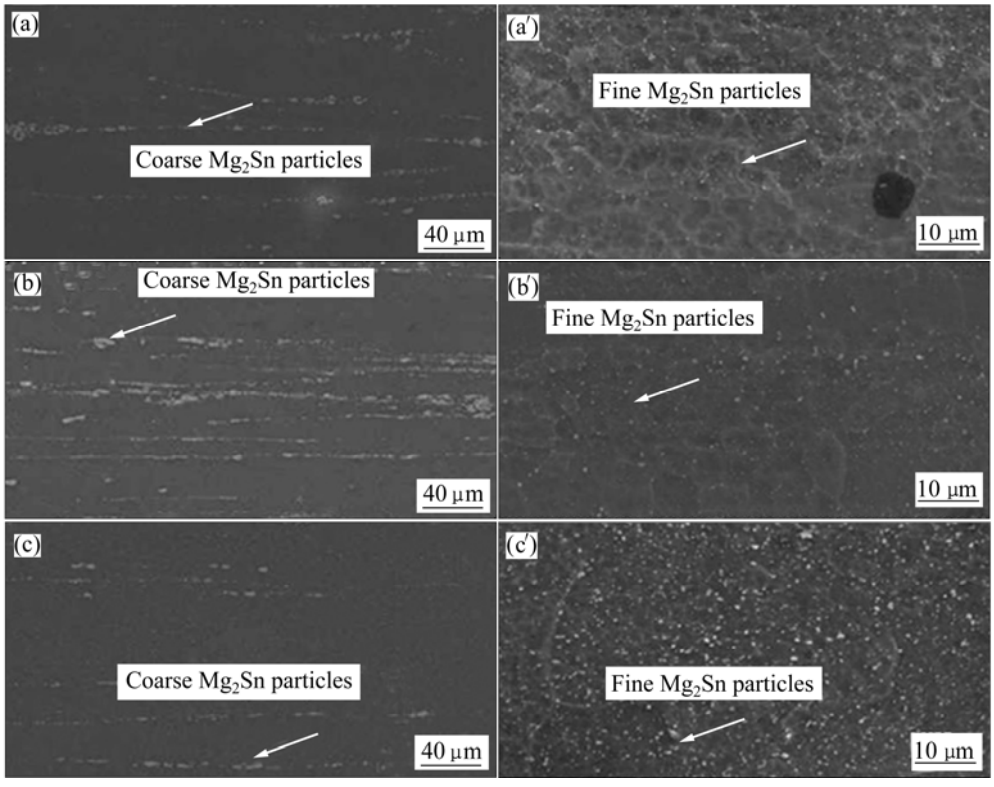

Fig. 3 SEM micrographs of extruded T10 alloys in different conditions: (a), (a′) T10-L; (b), (b′) T10-M; (c), (c′) T10-H

working temperature increases, with the values being 7.8% (T10-L), 6.5% (T10-M) and 11.6% (T10-H), respectively. Generally, an increase in working temperature results in enhanced atom diffusion ability and thus enhanced precipitation kinetics, namely higher precipitation ability. Therefore, the area fraction of FMPs of T10-H alloys is the highest. For the case of T10-M alloy, the higher area fraction of CMPs consumes certain amount of Sn, therefore, the area fraction of FMPs is reduced because the total Sn content is fixed. Some fine particles located on grain boundaries would restrain the migration of grain boundaries, which is one of the main reasons for obtaining the homogeneous fine-grained microstructure in T10 extruded alloys.

Textures measured by the X-ray technique are presented in the form of inverse pole figures (IPFs). Figure 4 shows the IPFs of extruded alloys. All IPFs reveal a fiber type texture [5, 7] in which $[10\bar{1}0]$ crystal orientation is preferentially parallel to the extrusion direction. The texture is typical of the Mg alloy extrusions resulted from a unidirectional deformation,

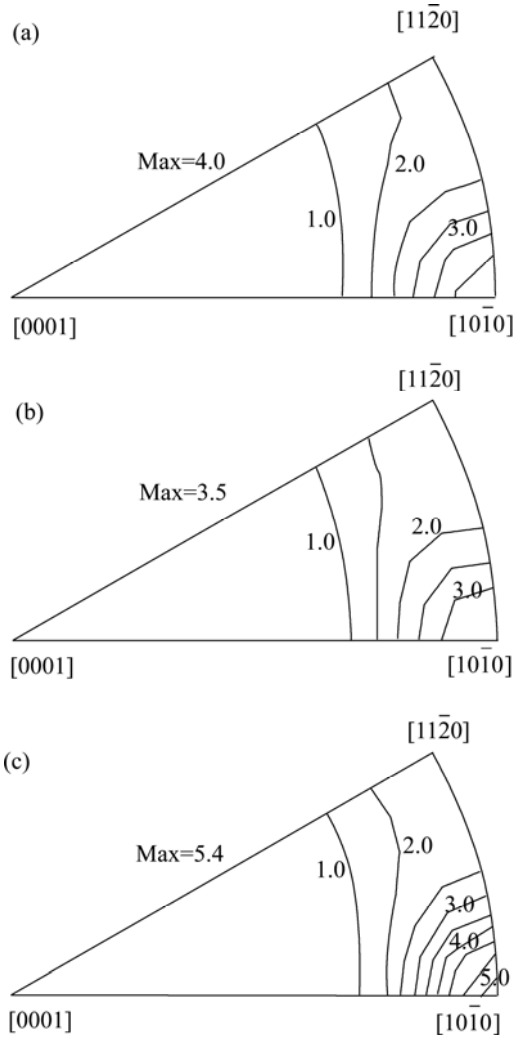

Fig. 4 Inverse pole figures of studied alloys referring to extrusion direction: (a) T10-L; (b) T10-M; (c) T10-H

recrystallization (dynamic and/or static) and possibly grain growth [14−15]. It is interesting to note that the variation in maximal texture intensities as a function of working temperature is similar with that of area fraction of CMPs. T10-M alloy with the highest area fraction of CMPs has the weakest texture. BALL and PRANGNELL [16] indicated that the coarse second-phase particles inside the stringers with micro-meter levels are effective in promoting dynamic recrystallization by providing potential nucleation site, known as particle-stimulated nucleation (PSN). And PSN offers a way to alter or weaken the texture. Therefore, the present T10-M alloy with most coarse particles exhibits the weakest texture. Without any doubt, the contribution of RSGs to the texture weakening in T10-M alloy should not be neglected.

It was reported that recrystallization mechanisms can be divided, according to the nature of the recrystallization process, into two groups: continuous dynamic recrystallization (CDRX) and discontinuous dynamic recrystallization (DDRX) [17]. CDRX grains nucleated at the mobile dislocations trapping place [18]. DDRX grains nucleated at the bugles between original grain and the neighboring grains [19]. More recently, BARNETT [15] reported that $[10\bar{1}0]$ fiber texture arises partly from the tendency of individual grains to deform in a manner closer to plane strain instead of axisymmetrically. BARNETT [15] also realized that orientations of recrystallization nuclei can dominate the bulk texture following recrystallization and grain growth. It can be concluded that the orientations of the recrystallization nuclei must be different form those of CDRX nuclei. In addition, CDRX often occurred at medium deformation temperature while that of DDRX was higher. From the results mentioned above, it seems that differences in nucleation of new grains lead to the variation in texture intensity of the extruded T10-L and T10-H alloys. It is concluded that the nucleation of new grains in T10 alloys is associated with dislocations/twin trapping, grain boundary bulging and PSN (leading to basal texture weakening).

Figure 5 shows the tensile stress−strain curves of the T10 alloys in different conditions. Related mechanical properties are summarized in Table 2. All the stress−strain curves have a special characteristic in common. They all reveal a flow stress maximum followed by a conspicuous loss of strength. The variation in working temperature can influence the tensile properties of the alloys greatly. The tensile strength of T10-H is the highest, but the stress decreases rapidly during the deformation, resulting in a smaller elongation to failure, which stems from the strong texture [20]. Among the specimens investigated, T10-M shows the poorest tensile properties and lowest work hardening rate.

For the case of T10-L and T10-M alloys, as the working temperature increases, both strength and ductility deteriorate, which is different from the typical relationship between strength and ductility. The decrease in strength with increasing working temperature is mainly due to reduced grain boundary strengthening, following the Hall-Petch relationship. The decrease in ductility is ascribed to the higher fraction of stringers of the CMPs. Previous report [8] indicated that these coarse particles may become a site for crack nucleation during tensile test, and thus result in a poor ductility. Note that on the stress−strain curves, work hardening is followed by an apparently steady-state deformation behavior with a nearly constant flow stress. Generally, such a steady-state deformation is considered to occur by a dynamic balance between hardening and softening effect.

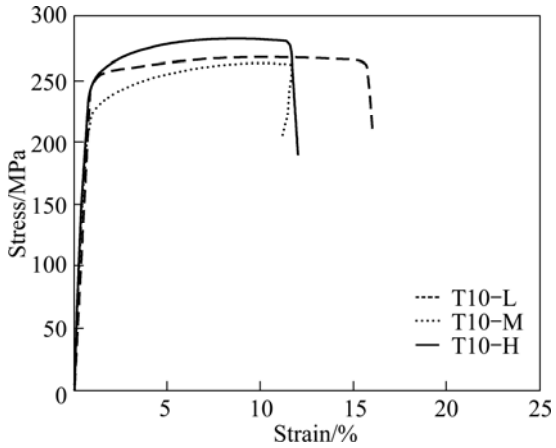

Fig. 5 Tensile stress−strain curves of extruded T10 alloys

For the case of T10-L and T10-H alloys, the grain sizes are 2.0 μm and 15.2 μm, respectively. Generally, tensile yield strength (TYS) increases significantly with decreasing the grain size. On the contrary, for the case studied here, the grain size dependence of tensile strength is not recognized as the grain size exceeds 15 μm. The strength of the alloy is mainly determined by contribution of texture strengthening and particle strengthening. Owing to the strong basal texture of T10-H alloy, as shown in Fig. 4, when the stress axis is parallel to the extrusion direction, the normal direction of the most basal slip planes is nearly perpendicular to the stress axis. Thus, the ideal Schmid factor for basal slip is zero in the sample T10-H [20]. Furthermore, YUAN et al [21] indicated that stronger basal texture/hard orientation (difficult activation for basal slip) leads to higher friction stress, namely better strengthening. Precipitates of metastable transition or equilibrium phases are often key strengthening constituents in many magnesium alloys [22]. Granular FMPs could effectively impede microcrack and dislocation movement, therefore strengthening the alloy. To sum up, the high strength of T10-H alloy is mainly due to the particle strengthening and texture strengthening mechanisms resulted from the more and finer primarily dispersed particles and stronger texture, respectively.

4 Conclusions

1) Grain size, texture and dynamic recrystallization mechanism are found to be significantly influenced by the working temperature, resulting in fine grain size at a low temperature, and strong texture at a high temperature.

2) The texture intensity variation with working temperature is associated with the difference in the nucleation of new grains at different working temperatures. It is concluded that the nucleation of new grains in T10 alloys is associated with dislocations/twin trapping, grain boundary bulging and PSN (leading to basal texture weakening).

3) For the cases of T10-L and T10-M alloys, the grain boundary strengthening is the main strengthening mechanism. As the grain size exceeds 15 μm, particle strengthening and texture strengthening are the main strengthening mechanisms. Among alloys tested, the T10-H alloy with the strongest basal texture has the largest tension yield strength (240 MPa).

References

[1] UEMATSU Y, TOKAJI K, KAMAKURA M, UCHIDA K, SHIBATA H, BEKKU N. Effect of extrusion conditions on grain refinement and fatigue behavior in magnesium alloys [J]. Mater Sci Eng A, 2006, 434: 131−140.

[2] MENDIS C L, OHISHI K, KAWAMURA Y, HONMA T, KAMADO S, HONO K. Precipitation-hardenable Mg–2.4Zn–0.1Ag–0.1Ca–0.16Zr (at.%) wrought magnesium alloy [J]. Acta Mater, 2009, 57: 749−760.

[3] YAMASHITA A, HORITA A, LANGDON T G. Improving the mechanical properties of magnesium and a magnesium alloy through severe plastic deformation [J]. Mater Sci Eng A, 2001, 300: 142−147.

[4] MUKI T, HIGDSHI K. Ductility enhancement of ultra fine-grained aluminum under dynamic loading [J]. Scripta Mater, 2001, 44: 1493−1496.

[5] KIM H K, LEE Y I, CHUNG C S. Fatigue properties of a fine-grained magnesium alloy produced by equal channel angular pressing [J]. Scripta Mater, 2005, 52: 473−477.

[6] SASAKI T T, YAMAMOTO K, HONMA T, KAMADO S, HONO K. A high-strength Mg-Sn-Zn-Al alloy extruded at low temperature [J]. Scripta Mater, 2008, 59: 1111−1114.

[7] PARK S S, TANG W N, YOU B S. Microstructure and mechanical properties of an indirect-extruded Mg-8Sn-1Al-1Zn alloy [J]. Mater Letters, 2010, 64: 31−34.

[8] CHENG W L, PARK S S, YOU B S, KOO B H. Microstructure and mechanical properties of binary Mg-Sn alloys subjected to indirect extrusion [J]. Mater Sci Eng A, 2010, 527: 4250−4253.

[9] KANG D H, PARK S S, KIM N J. Development of creep resistant die cast Mg-Sn-Al-Si alloy [J]. Mater Sci Eng A, 2005, 413−414: 555−560.

[10] MENDIS C L, BETTLES C J, GIBSON M A, HUTCHINSON C R. An enhanced age hardening response in Mg-Sn based alloys containing Zn [J]. Mater Sci Eng A, 2006, 435/436: 163−171.

[11] LIU H, CHEN Y, TANG Y, HUANG D, NIU G. The microstructure and mechanical properties of permanent-mould cast Mg−5wt%Sn−(0−2.6)wt%Di alloys [J]. Mater Sci Eng A, 2006, 437: 348−355.

[12] PARK S S, YOU B S, YOON D J. Effect of the extrusion conditions on the texture and mechanical properties of indirect-extruded Mg-3Al-1Zn alloy [J]. J Mater Processing Tech, 2009, 209: 5940−5943.

[13] SHAHZAD M, WAGNER L. Influence of extrusion parameters on microstructure and texture developments, and their effects on mechanical properties of the magnesium alloy AZ80 [J]. Mater Sci Eng A, 2009, 506: 141−147.

[14] AZEEM M A, TEWARI A, MISHRA S, GOLLAPUDI S, RAMAMURTY U. Development of novel grain morphology during hot extrusion of magnesium AZ21 alloy [J]. Acta Mater, 2010, 58: 1495−1502.

[15] BARNETT M R, SULLIVAN A, STANFORD N, BEER A. Texture selection mechanisms in uniaxially extruded magnesium alloys [J]. Scripta Mater, 2010, 63: 721−724.

[16] BALL E A, PRANGNELL P B. Tensile-compressive yield asymmetries in high strength wrought magnesium alloys [J]. Scripta Mater, 1994, 31: 111−116.

[17] NIE J F. Effects of precipitate shape and orientation on dispersion strengthening in magnesium alloys [J]. Scripta Mater, 2003, 48: 1009−1015.

[18] AL-SAMMAN T, GOTTSTEIN G. Dynamic recrystallization during high temperature deformation of magnesium [J]. Materials Science and Engineering A , 2008, 490: 411−420.

[19] LIU C M, LIU Z J, ZHU X R, ZHOU H T. Research and development progress of dynamic recrystallization in pure magnesium and its alloys [J]. The Chinese Journal of Nonferrous Metals, 2006, 16: 1−12. (in Chinese)

[20] CHANG L L, WANG Y N, ZHAO X, HUANG J C. Microstructure and mechanical properties in an AZ31 magnesium alloy sheet fabricated by asymmetric hot extrusion [J]. Mater Sci Eng A, 2008, 496: 512−516.

[21] YUAN W, PANIGRAHI S K, SU J Q, MISHRA R S. Influence of grain size and texture on Hall−Petch relationship for a magnesium alloy [J]. Scripta Materialia, 2011, 65: 994−997.

[22] YUAN G Y, SUN Y S, DING W J. Effect of Sb addition on the microstructure and mechanical properties of AZ91 magnesium alloy [J]. Scripta Materialia, 2000, 43(11): 1009−1013.

(Edited by YANG Bing)